



HAL
open science

Atmospheric pressure generation of O(a) by microplasmas

J.S. Sousa, G. Bauville, B. Lacour, V. Puech, M. Touzeau

► **To cite this version:**

J.S. Sousa, G. Bauville, B. Lacour, V. Puech, M. Touzeau. Atmospheric pressure generation of O(a) by microplasmas. *European Physical Journal: Applied Physics*, 2009, 47 (2), pp.1-7. 10.1051/ep-jap/2009103 . hal-00489489

HAL Id: hal-00489489

<https://hal.science/hal-00489489>

Submitted on 5 Jun 2010

HAL is a multi-disciplinary open access archive for the deposit and dissemination of scientific research documents, whether they are published or not. The documents may come from teaching and research institutions in France or abroad, or from public or private research centers.

L'archive ouverte pluridisciplinaire **HAL**, est destinée au dépôt et à la diffusion de documents scientifiques de niveau recherche, publiés ou non, émanant des établissements d'enseignement et de recherche français ou étrangers, des laboratoires publics ou privés.

ATMOSPHERIC PRESSURE GENERATION OF $O_2(a^1\Delta_g)$ BY MICROPLASMAS

Santos Sousa J.^{a,b}, Bauville G.^a, Lacour B.^a, Puech V.^a and Touzeau M.^c

a) *Laboratoire de Physique des Gaz et des Plasmas (UMR 8578, CNRS & Université Paris-Sud, Bâtiment 210, 91405 Orsay, FRANCE)*

b) *Instituto de Plasmas e Fusão Nuclear (Instituto Superior Técnico, Avenida Rovisco Pais, 1049-001 Lisboa, PORTUGAL)*

c) *Laboratoire des Techniques de la Microélectronique (UMR 5129, CNRS & Université Joseph Fourier & INPG, 17 Avenue des martyrs, 38054 Grenoble, FRANCE)*

PACS numbers: 52.50.Dg, 52.70.Kz, 52.80.Tn

Abstract. The generation of singlet oxygen states ($O_2(a^1\Delta_g)$) by microplasmas has been studied experimentally. In the present paper, it is shown that micro-cathode sustained discharges (MCSD's) can be used to produce high fluxes of $O_2(a^1\Delta_g)$ at atmospheric pressure. In He/ O_2 /NO mixtures, $O_2(a^1\Delta_g)$ number densities higher than 10^{16} cm^{-3} can be generated by this 3-electrode configuration and transported over distances of some tens of cm. In fact, at total flow rates up to 30 l/min, $O_2(a^1\Delta_g)$ fluxes above 10 mmol/h were measured in the MCSD afterglow, at 26 cm downstream. As a result, MCSD's appear to be very efficient and suitable tools for the continuous production of large amounts of $O_2(a^1\Delta_g)$ at atmospheric pressure, which could give rise to a wide range of new applications, namely biological. The effect of different parameters such as gas flows and mixtures, and discharge current are discussed in the paper.

1. INTRODUCTION

Singlet delta oxygen, $O_2(a^1\Delta_g)$, the first electronically excited low-energy (0.98 eV) state of molecular oxygen, possesses an extremely long radiative lifetime of more than 73 min. Moreover, this metastable state of molecular oxygen is very resistant against homogeneous and heterogeneous relaxation processes, which makes it possible for $O_2(a^1\Delta_g)$ to be used far away from its place of production. As so, this unique molecular state can be used as an energy donor for a large spectrum of applications, including removal of air pollutants [1], degradation of synthetic polymers [2], medicine [3], laser excitation [4], or combustion [5]. Furthermore, $O_2(a^1\Delta_g)$ is also well known to produce cytotoxic effects and to be an important agent in biophysical and biochemical processes [6-11]. Up to now, for biological applications, $O_2(a^1\Delta_g)$ is mainly produced through the photosensitization technique [11] resulting in rather low $O_2(a^1\Delta_g)$ concentrations, of a few hundreds parts per billion, in gas flow at atmospheric pressure [12]. Thus, new plasma sources of high fluxes of $O_2(a^1\Delta_g)$ molecules are of high potential interest for biological applications, but at the mandatory condition that these sources can be operated at atmospheric pressure and the $O_2(a^1\Delta_g)$ can be transported to targets placed at some tens of cm from the source.

While it is well known for many years that $O_2(a^1\Delta_g)$ can be efficiently produced in oxygen discharges operating at a pressure of few mbars [13], its production by high pressure discharges, and specifically at atmospheric pressure, is still very challenging, as described in the comprehensive topical review about the physics and the engineering of $O_2(a^1\Delta_g)$ production in low temperature plasma, recently published by Ionin et al [14]. In the previous years, the production of $O_2(a^1\Delta_g)$ by high pressure electrical discharges has attracted much attention because of its potential application for the pumping

^a Electronic address: joao.santos-sousa@u-psud.fr

of the oxygen-iodine laser [15-19]. In order to efficiently produce the high $O_2(a^1\Delta_g)$ densities needed for these applications, it is now established that an electric discharge source must satisfy two conditions: i) it must be stable at high pressure and high power loading and ii) it should operate at low reduced electric field [20]. So far, high-pressure, non-self-sustained discharges operating in short duration pulsed mode seemed to be the most attractive option for generating stable discharges at high pressure. Different kinds of non-self sustained discharges have been extensively investigated for $O_2(a^1\Delta_g)$ production: i) the e-beam sustained discharges [14,17,21], ii) the crossed spiker-sustainer discharges [22,23], and iii) the controlled avalanche method [24]. However, we have recently demonstrated [25] that the so-called micro-cathode sustained discharge (MCSD), operating in DC mode, can also be used to produce large amounts of $O_2(a^1\Delta_g)$. Detailed numerical simulations of the MCSD [26,27] have shown that the MCSD is basically a high pressure positive column with a low value of the reduced electric field and gas temperature. It must be pointed out that, to this date, the MCSD is the only DC discharge technique which has been proven capable of generating high $O_2(a^1\Delta_g)$ concentrations at atmospheric pressure [28,29]. As shown by modeling and experiments [30-32], the MCSD exhibits unrivalled discharge stability properties which directly result from the stability of the micro-hollow cathode discharge (MHCD) which acts as a plasma cathode in such a device [33,34]. The stability of the MHCD results from the transition from an abnormal discharge mode, which occurs at low current when the discharge is confined inside the hole of the MHCD, to a normal discharge mode, characterized by a plasma extension on the backside of the MHCD cathode, as the current increases [35-37]. As a result, this transition prevents, at high pressure and current, the development of the classical thermal instability which induces the discharge constriction and the glow to arc transition in many kinds of discharges.

2. EXPERIMENTAL SET-UP

As shown in **Figure 1**, our microplasma reactor basically consists of a micro-hollow cathode discharge (MHCD), a discharge concept first developed by Schoenbach and co-workers [38], acting as a plasma cathode to generate a stable glow discharge of larger volume between the MHCD and a third, 2.5 cm diameter, planar electrode, placed at a distance of 8 mm from the MHCD. This 3-electrode configuration is the so-called MCSD, which was initially proposed by Stark and Schoenbach [33,34]. The MHCD itself was made of 100 μm thick molybdenum electrodes glued on each side of a 500 μm thick alumina plate. An 800 μm diameter hole was pierced through this sandwich. The MHCD cathode is connected to a negative power supply through a 440 k Ω resistor, while the MHCD anode (anode A1) is directly grounded. Facing the anode A1 is the third electrode (anode A2), which is positively biased through a 440 k Ω resistor. The device is placed into a stainless steel chamber, which is evacuated down to 10^{-3} Torr before the gas mixture is introduced. The total pressure in the chamber is measured with a Baratron gauge, while the helium, oxygen and nitric oxide (NO) flows are separately regulated with flow-meters. Optical windows (not shown in **Figure 1**) allow CCD imaging of the spatial discharge development and optical emission spectroscopy.

After passing through the discharge chamber, the gas flow is evacuated through a pumping line. A calibrated detection cell equipped with quartz windows can be positioned at different locations on the pumping line, allowing the measurement of the radiative emission of $O_2(a^1\Delta_g)$ at 1.27 μm . This emission provides a measure of the $O_2(a^1\Delta_g)$ number density in the flowing afterglow. The distance between this cell and the discharge reactor can be varied in the range 20-70 cm. The detection system consists of a calibrated liquid-nitrogen-cooled InGaAs detector (Judson model J22D-M204) and a narrow band (19 nm) interference filter centred at 1.27 μm . The signal is amplified by an op-amp with a gain of 10^7 and monitored with a numerical oscilloscope, which is also used to record the electrical parameters of the discharge. A part of the infrared emission is picked up with an optical fiber connected to a spectrometer equipped with a 512 pixel InGaAs detector (OMA-V from Roper Scientific). **Figure 2** presents a comparison between spectra recorded at 26 cm downstream in the afterglow with the MCSD operating in pure oxygen at a pressure of 9 mbar and a discharge current of 2 mA (**Figure 2 (a)**) and in a He/ O_2 /NO mixture at atmospheric pressure (2.2% of O_2 and 185 ppm of NO) with a discharge current of 5 mA (**Figure 2 (b)**). Even if the $O_2(a^1\Delta_g)$ number density is 25 times

higher in the case of the He/O₂/NO mixture at atmospheric pressure ($9.8 \cdot 10^{15} \text{ cm}^{-3}$) than in the case of the low pressure of pure oxygen ($3.8 \cdot 10^{14} \text{ cm}^{-3}$), the comparison of the normalized spectra points out that they are essentially the same, in spite of the very different discharge conditions. This insures that, in He/O₂/NO mixtures, the infrared signal measured in the flowing afterglow is only due to the radiative emission of O₂(a¹Δ_g) and is not contaminated by spurious signals originating either from important collision-induced emission or NO*₂ de-excitation, which could add continua to the O₂(a¹Δ_g) spectrum. Therefore, the signal measured by the Judson detector can be used with confidence to measure the O₂(a¹Δ_g) density. Knowing the sensitivity of the detector, the transmission curve of the interference filter, the geometrical parameter of the optical detection system, and the radiative transition probability of O₂(a¹Δ_g), ($A=2.256 \cdot 10^{-4} \text{ s}^{-1}$) [39], the absolute O₂(a¹Δ_g) number density can be deduced from the amplitude of the infrared signal. In that procedure, a Monte Carlo simulation was used to calculate the probability that a photon emitted in the detection cell will reach the InGaAs element of the Judson detector. As a result, in our device, the O₂(a¹Δ_g) number density is correlated to the intensity of the Judson signal by the ratio $3.77 \cdot 10^{15} \text{ O}_2(\text{a}^1\Delta_g) \text{ cm}^{-3} / \text{mV}$.

The measurement of the ozone (O₃) number density is based on ultraviolet (UV) absorption. As a UV source we used a deuterium lamp emitting a broadband spectrum between 180 and 400 nm. In the present work, the measurements were mainly performed by using the calibrated detection cell, 8 cm long, as an absorption cell. However, in some experiments a longer cell, 50 cm long, was used to get more accurate results at low O₃ density. The O₃ number density was deduced from the ratio of the intensity (I) transmitted when the discharge is ON to the intensity (I₀) transmitted when the discharge is OFF. The O₃ density is deduced from the relation

$$\ln(I_0/I) = [\text{O}_3] \cdot \sigma \cdot L \quad (1),$$

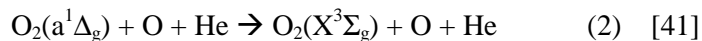
where σ is the absorption cross-section and L is the length of the absorption path. The O₃ absorption cross-section was measured by Molina and Molina [40]. After passing through the absorption cell, the transmitted light intensity is detected with a 75 cm focal length spectrometer (Acton 2750) and a 1340 pixel detector (Pixis from Roper Scientific) providing a resolution of 0.044 nm per pixel in the UV range. **Figure 3** shows the variation of $\ln(I_0/I)$ versus wavelength in the range 220-270 nm, for a discharge operating in a He/O₂ mixture (1% of O₂) at atmospheric pressure with a current of 3 mA. From the absorption cross-section given in [40], an O₃ density of $2.15 \pm 0.06 \cdot 10^{15} \text{ cm}^{-3}$ was obtained over all the wavelength range. For the different experimental conditions of the present work, we measured intensity values integrated between 253 and 255 nm, and we recorded the temporal evolution of these values with the discharge alternatively ON and OFF, as shown in **Figure 4**. As a result, O₃ number densities in the range 10^{13} - 10^{16} cm^{-3} were measured.

The O₂(a¹Δ_g) and O₃ number densities presented in this paper were measured in the MCSD afterglow, at 26 cm downstream.

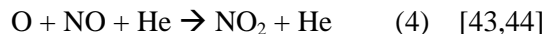
3. RESULTS AND DISCUSSION

The O₂(a¹Δ_g) number density is a very sensitive function of the gas velocity, due to the occurrence of fast quenching processes. In fact, the O₂(a¹Δ_g) molecules are presumably quenched by atomic oxygen (O-atom) and O₃ for long residence time [14,41]. Therefore, the higher the gas flow, the lower the destruction of the O₂(a¹Δ_g) states before their detection in the afterglow, as pointed out by **Figure 5**. Actually, for binary He/O₂ mixtures at atmospheric pressure, the MCSD allowed the production of an O₂(a¹Δ_g) density of about 10^{15} cm^{-3} whenever the helium flow was higher than 15000 sccm. In order to get greater O₂(a¹Δ_g) concentrations, we could increase the oxygen flow. However, this can't be done endlessly due to insufficient energy deposition per oxygen molecule, P/Q, for higher oxygen flows. Thus, as shown in **Figure 5**, besides the helium flow, the O₂(a¹Δ_g) generation is maximized whenever the oxygen concentration is about 1-2%.

In these experimental conditions, characterized by atmospheric pressure and low oxygen partial pressure, the main O₂(a¹Δ_g) destruction channel is expected to be the three-body reaction:

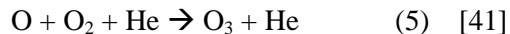


Thereby, one solution to increase the $\text{O}_2(a^1\Delta_g)$ number density is to add, in the He/ O_2 mixture, an O-atom scavenger in order to reduce the quenching processes. As so, we have studied the influence of adding NO molecules at low concentration in the He/ O_2 mixture at atmospheric pressure. As pointed out by **Figures 6** and **7**, adding small concentrations of NO induces, on the one hand, a large increase of the $\text{O}_2(a^1\Delta_g)$ number density (up to 50 times more), and, on the other hand, a huge reduction on the O_3 number density (up to its apparent complete destruction). As shown in **Figure 8**, the O_3 molecules and the O-atoms are quenched by NO through the reactions:

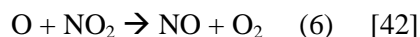


So, the observed increase in the $\text{O}_2(a^1\Delta_g)$ density probably results from a decrease in the O-atom and O_3 densities. In fact, the $\text{O}_2(a^1\Delta_g)$ states are expected to be quenched by the O-atoms in the discharge and by the O_3 molecules in and after the discharge. Since the effect of NO is to quench the O-atom and the O_3 , injecting NO in the gas flow is likely to reduce the loss of $\text{O}_2(a^1\Delta_g)$ molecules. However, this assumption remains to be validated by measurements of the O-atom and NO_x densities, in the discharge chamber and in the afterglow, and for different discharge conditions. We intend to make these measurements by using, for the O-atom density, either the NO titration method or the two photon laser-induced fluorescence technique, as we have already done for MCSD operating in pure oxygen [26], and, for the NO_x density, through the UV absorption approach or the Fourier transform infrared spectroscopy technique.

In **Figures 6** and **7**, we observe that the huge reduction on the O_3 number density is much greater than the small concentration of NO added. Indeed, as pointed out by **Figure 7 (a)**, by only introducing 0.15 sccm of NO in the gas mixture, the O_3 is presumably totally destroyed, with its density passing from $3.0 \cdot 10^{15} \text{ cm}^{-3}$ to less than $1.0 \cdot 10^{13} \text{ cm}^{-3}$ (under the limit of detection). As previously mentioned, besides destroying O_3 , the NO also quenches O-atom. With increasing pressure, O_3 starts to be produced effectively in a three-body recombination of atomic and molecular oxygen (see **Figure 8**):



This is especially true at atmospheric pressure, when almost all O-atom becomes O_3 [45,46]. So, a reduction in the O-atom density also leads to a decrease in the O_3 density in the gas flow. Furthermore, as NO is not lost in the process, but it is rather recycled in collisions (see **Figure 8**)



the earlier referred effects and reactions are somehow catalytic and, thus, cause a huge decrease on the O_3 density.

On the other hand, in **Figures 6 (a)** and **7 (a)**, the increase of the $\text{O}_2(a^1\Delta_g)$ number density is much larger than the initial concentration of O_3 (for $Q(\text{NO}) = 0$ sccm). As clearly pointed out by **Figure 6 (b)** and **7 (b)**, the increase of the $\text{O}_2(a^1\Delta_g)$ density is strongly correlated with the reduction of the O_3 density. As a matter of fact, the rise of the number of $\text{O}_2(a^1\Delta_g)$ molecules is equal to the decrease found on the number of O_3 molecules. Actually, this is also observed in **Figures 6 (a)** and **7 (a)**, as the increase of the $\text{O}_2(a^1\Delta_g)$ density until the O_3 complete destruction is equal to the O_3 initial concentration. The further increase of the $\text{O}_2(a^1\Delta_g)$ density can only be explained by a decrease on the O-atom density and a consequent reduction of the $\text{O}_2(a^1\Delta_g)$ molecules loss. The stabilization of the $\text{O}_2(a^1\Delta_g)$ density for higher NO flow could mean that there are no more O-atom to be quenched. But, as already mentioned, these hypotheses need to be verified by measuring the O-atom density in and after the discharge. Besides that, NO and NO_2 molecules also having a quenching effect on $\text{O}_2(a^1\Delta_g)$ can induce as well a stabilization of the $\text{O}_2(a^1\Delta_g)$ density. Moreover, a decrease of the $\text{O}_2(a^1\Delta_g)$ density is expected for greater concentrations of NO. Indeed, a reduction of the number of $\text{O}_2(a^1\Delta_g)$ molecules with increasing flow of NO has been observed for other discharge conditions [29]. Therefore, the optimum NO gas flow is a sensitive function of both the oxygen partial pressure and the helium flow.

From **Figures 6** and **7**, we can also infer about the influence of the helium flow and the oxygen partial

pressure on the $O_2(a^1\Delta_g)$ and O_3 densities. For a constant oxygen partial pressure, the $O_2(a^1\Delta_g)$ initial density (for $Q(NO) = 0$ sccm) is larger when the helium flow is higher (while no difference is observed for O_3 number density). But the increase, versus the NO concentration, of the $O_2(a^1\Delta_g)$ density is smaller as the helium flow is higher. A greater gas flow means a shorter transit time and, thus, a reduction of the quenching effect before reaching the detection cell. This immediately explains the increase observed for the $O_2(a^1\Delta_g)$ initial densities. As the O-atom and the O_3 are also less quenched by NO for higher gas flow, the addition of small concentrations of NO becomes less effective in increasing the $O_2(a^1\Delta_g)$ number density. Even if we do not have measurements of the O-atom density, **Figures 6** and **7** demonstrate that the reduction of the O_3 density with increasing NO flow is less important for higher gas flow. As shown in **Figures 6 (b)** and **7 (b)**, for a constant helium flow, besides the decrease of the energy deposited per oxygen molecule, P/Q , we do not notice large differences with increasing oxygen partial pressure, apart from the O_3 initial density. The increase of the O_3 density with higher oxygen concentration is expected as O_3 is effectively produced through the reaction (5). To clearly understand the influence of the helium flow and the oxygen partial pressure on the $O_2(a^1\Delta_g)$ density, we should observe **Figure 9**.

As pointed out by **Figure 9**, for a discharge current of 3 mA, the largest $O_2(a^1\Delta_g)$ densities are obtained for helium flows of about 6000 sccm, regardless of the oxygen partial pressure. The maximal $O_2(a^1\Delta_g)$ density, of about $7.5 \cdot 10^{15} \text{ cm}^{-3}$, was observed for an oxygen partial pressure of 20 mbar. The shape of the curves showed in **Figure 9** results from a competition between two effects. Increasing the total flow leads, on the one hand, to a decrease of the residence time in the afterglow, and, on the other hand, to a decrease of the residence time in the discharge and to an increase of the oxygen flow. The first effect causes a reduction of the losses of $O_2(a^1\Delta_g)$ during transport. The last two effects induce a decrease of the P/Q , resulting in a reduction of the production of $O_2(a^1\Delta_g)$. For a given oxygen partial pressure, i.e. a given oxygen gas flow, the P/Q value can be increased by increasing the discharge current. **Figure 10** shows that, for oxygen and NO partial pressures respectively equal to 23 and 0.19 mbar the $O_2(a^1\Delta_g)$ number density increase is nearly linear for discharge currents up to 5 mA, while at higher currents the $O_2(a^1\Delta_g)$ density begins to saturate. As a result, $O_2(a^1\Delta_g)$ number densities higher than $1.0 \cdot 10^{16} \text{ cm}^{-3}$ have been produced by MCSD operating at atmospheric pressure.

4. CONCLUSIONS

In the present paper, we have shown that the MCSD's can be efficiently used to generate stable DC glow discharges, free from the glow-to-arc transition, at atmospheric pressure in binary He/ O_2 and ternary He/ O_2 /NO mixtures. Our results show that $O_2(a^1\Delta_g)$ number densities higher than 10^{16} cm^{-3} can be obtained at atmospheric pressure and transported over some tens of cm for helium flows in the range 2000-30000 sccm. It should be emphasized that the densities of the various excited states, $O_2(a^1\Delta_g)$ and O_3 , impacting targets positioned up to 50 cm downstream are very reproducible. Throughout the course of experiments performed during several months, the variation of the $O_2(a^1\Delta_g)$ and O_3 concentrations is lower than 10%, for given values of gas flows and discharge current. Moreover, it should be pointed out that the ratio between the $O_2(a^1\Delta_g)$ and the O_3 densities can be finely tuned through the values of the discharge current and the NO concentration. Thus, MCSDs operating at atmospheric pressure in He/ O_2 /NO mixtures appear to be very suitable tools for different applications, and particularly for biological ones [47].

ACKNOWLEDGMENTS

This work was partially supported by the French Agence Nationale de la Recherche. J.S.S thanks the Portuguese Fundação para a Ciência e a Tecnologia (Grant No. SFRH/28668/2006) for their financial support.

REFERENCES

- [1] J.N. Pitts, *Adv. Environ. Sci.* **1**, 289 (1969)
- [2] J.F. Rabek, R.J. Ranby, *Polym. Eng. Sci.* **15**, 40 (1975)
- [3] T.J. Dougherty, J.E. Kaufman, A. Goldfarb, K.R. Weishaupt, D. Boyle, A. Mittleman, *Cancer Res.* **38**, 2828 (1978)
- [4] W.E. McDermott, N.R. Pchelkin, D. Benard, R. Bousek, *Appl. Phys. Lett.* **32**, 469 (1978)
- [5] A.M. Starik, N.S. Titova, *Dokl. Phys.* **46**, 627 (2001)
- [6] N.I. Krinsky, in *Singlet Oxygen*, edited by H.H. Wasserman and R.W. Murray (Academic Press, New York, 1979)
- [7] A.A. Frimer (ed), *Singlet O₂*, vol. 4, CRC Press Boca Raton, FL (1985)
- [8] L. Packer, H. Sics (eds.), *Methods in Enzymology*, vol. 319: "singlet oxygen, UV A and ozone", Academic Press (2000)
- [9] H. Tatsuzawa, T. Maruyama, N. Misawa, K. Fujimori, K. Hori, Y. Sano, Y. Kambayashi, M. Nakano, *FEBS Lett.* **439**, 329 (1998)
- [10] J.L. Ravanat, G.R. Martinez, M.G.H. Medeiros, P. Di Mascio, J. Cadet, *Tetrahedron* **62**, 10709 (2006)
- [11] W. R. Midden, S.Y. Wang, *J. Am. Chem. Soc.* **105**, 4129 (1983)
- [12] L.J. Schiff, W.C. Eisenberg, J. Dziuba, K. Taylor, S.J. Moore, *Environ. Health Perspectives.* **76**, 199 (1987)
- [13] G. Gousset, P. Panafieu, M. Touzeau, M. Vialle, *Plasma Chem. Plasma Process.* **7**, 409 (1987)
- [14] A.A. Ionin, I.V. Kochetov, A.P. Napartovich, N.N. Yuryshev, *J. Phys. D: Appl. Phys.* **40**, R25 (2007)
- [15] A.P. Napartovitch, A.A. Deryugin, I.V. Kochetov, *J. Phys. D: Appl. Phys.* **34**, 1827 (2001)
- [16] J. Schmiedberger, H. Fujii, *Appl. Phys. Lett.* **78**, 2649 (2001)
- [17] A.A. Ionin, Yu. Klimachev, A.A. Kochetov, A.P. Napartovitch, L.V. Seleznev, D.V. Sinitsyn, G.D. Hager, *J. Phys. D: Appl. Phys.* **36**, 982 (2003)
- [18] D.S. Stafford, M.J. Kushner, *J. Appl. Phys.* **96**, 2451 (2004)
- [19] A.N. Vasiljeva, K.S. Klopovskiy, A.S. Kovalev, D.V. Lopaev, Y.A. Mankelevich, N.A. Popov, A.T. Rakhimova, T.V. Rakhimova, *J. Phys. D: Appl. Phys.* **37**, 2455 (2004)
- [20] A. Hill, in *Proceedings of the International Conference on LASERS, 2000*, edited by V. Corcora (STS, McLean, VA2000)
- [21] N.P. Vagin, A.A. Ionin, Yu. Klimachev, A.A. Kotkov, I.V. Kochetov, A.P. Napartovitch, Yu. Podmar'kov, L.V. Seleznev, D.V. Sinitsyn, M.P. Frolov, G.D. Hager, N.N. Yuryshev, *Quantum Electron.* **34**, 865 (2004)
- [22] A. Hicks, S. Norberg, P. Shawcross, W.R. Lampert, J.W. Rich, I.V. Adamovich, *J. Phys. D: Appl. Phys.* **38**, 3812 (2005)
- [23] A. Hicks, Yu.G. Utkin, W.R. Lempert, J.W. Rich, I.V. Adamovich, *Appl. Phys. Lett.* **89**, 241131 (2006)
- [24] A.E. Hill, *Appl. Phys. Lett.* **91**, 041116 (2007)
- [25] G. Bauville, B. Lacour, L. Magne, V. Puech, J.P. Boeuf, E. Munoz-Serrano, L.C. Pitchford, *Appl. Phys. Lett.* **90**, 031501 (2007)
- [26] G. Bauville, B. Lacour, L. Magne, V. Puech, J. Santos Sousa, J.P. Boeuf, G. Hagelaar, E. Munoz-Serrano, L.C. Pitchford, N. Sadeghi, M. Touzeau, in *Proceedings of the 38th AIAA Plasmadynamics and Lasers Conference, Miami, 2007*, AIAA paper 2007-4025
- [27] K. Makasheva, E. Munoz-Serrano, G. Hagelaar, J.P. Boeuf, L.C. Pitchford, *Plasma Phys. Control. Fusion* **49**, B233 (2007)
- [28] V. Puech, G. Bauville, B. Lacour, J. Santos Sousa, L.C. Pitchford, in *Proceedings of the SPIE International High Power Laser Ablation Symposium, Taos, 2008*, edited by C.R. Phipps (SPIE, 2008)
- [29] J. Santos Sousa, G. Bauville, B. Lacour, V. Puech, M. Touzeau, L.C. Pitchford, *Appl. Phys. Lett.* **93**, 011502 (2008)
- [30] K.H. Becker, K.H. Schoenbach, J.G. Eden, *J. Phys. D: Appl. Phys.* **39**, R55 (2006)
- [31] V. Puech, *Eur. Phys. J; Appl. Phys.* **42**, 17 (2008)

- [32] K. Makasheva, G. Hagelaar, J.P. Boeuf, Th. Callegari, L.C. Pitchford, IEEE Trans. Plasma Sci. **36**, 1236 (2008)
- [33] R.H. Stark, K.H. Schoenbach, Appl. Phys. Lett. **74**, 3770 (1999)
- [34] R.H. Stark, K.H. Schoenbach, J. Appl. Phys. **85**, 2075 (1999)
- [35] M.J. Kushner, J. Phys. D: Appl. Phys. **38**, 1633 (2005)
- [36] J.P. Boeuf, L.C. Pitchford, K.H. Schoenbach, Appl. Phys. Lett. **86**, 71501 (2005)
- [37] X. Aubert, G. Bauville, J. Guillon, B. Lacour, V. Puech, A. Rousseau, Plasma Sources Sci. Technol. **16**, 23 (2007)
- [38] K.H. Schoenbach, A. El-Habachi, W. Shi, M. Ciocca, Plasma Sources Sci. Technol. **6**, 468 (1997)
- [39] S.M. Newman, A.J. Orr-Ewing, D.A. Newnham, J.J. Ballard, J. Chem. Phys. A **104**, 9467 (2000)
- [40] L.T. Molina, M.J. Molina, J. Geo. Res. **91**, 14501 (1986)
- [41] O.V. Braginski, A.S. Kovalev, D.V. Lopaev, O.V. Proshina, T. V. Rakhimova, A.T. Rakhimova, A.N. Vasilieva, J. Phys. D: Appl. Phys. **40**, 6571 (2007)
- [42] R.A. Arakoni, N.Y. Babaeva, M.J. Kushner, J. Phys. D: Appl. Phys. **40**, 4793 (2007)
- [43] A. Hicks, J. Bruzzese, W.R. Lempert, J.W. Rich, I.V. Adamovich, in *Proceedings of the 38th AIAA Plasmadynamics and Lasers Conference, Miami, 2007*, AIAA paper 2007-4236
- [44] G.F. Benavides, D.M. Palla, A.D. King, D.L. Carroll, J.T. Verdeyen, J.K. Laystrom, T.H. Field, in *Proceedings of the 38th AIAA Plasmadynamics and Lasers Conference, Miami, 2007*, AIAA paper 2007-4623
- [45] K. Takezawa, R. Ono, T. Oda, in *Proceedings of the 40th IEEE - Industry Applications Society Annual Meeting, Hong Kong, 2005*, volume **4**, page 2914
- [46] B. Eliasson, U. Kogelschatz, IEEE Trans. Plasma Sci. **19**, 309 (1991)
- [47] J. Santos Sousa, G. Bauville, B. Lacour, V. Puech, M. Touzeau, J.L. Ravanat, in *Proceedings of the 61st Annual Gaseous Electronics Conference, Dallas, 2008*, Bull. Am. Phys. Soc., volume 53, number 10

Figure Captions

Figure 1: Schematic of the experimental set-up.

Figure 2: Infra-red spectra measured in the flowing afterglow (26 cm downstream from the MCSD) in a discharge operating (a) in pure O₂ at a pressure of 9 mbar and a discharge current of 2 mA, or (b) in a He/O₂/NO mixture at atmospheric pressure (2.2% of O₂ and 185 ppm of NO) and a discharge current of 5 mA.

Figure 3: Evolution of the absorbance versus the wavelength for a discharge operating at atmospheric pressure in a He/O₂ mixture (1% of O₂) and a discharge current of 3 mA.

Figure 4: Temporal evolution of the transmitted intensity of the deuterium lamp integrated from 253 to 255 nm. For times lower than 10 s or greater than 45 s, the discharge is OFF, while it is ON for times between 10 and 45 s. Upper red curve: He/O₂ mixture with 625 ppm of O₂ ; lower blue curve: He/O₂ mixture with 1% of O₂.

Figure 5: Evolution of the O₂(a¹Δ_g) number density versus the oxygen flow, obtained at atmospheric pressure, for a discharge current of 3 mA, in He/O₂ mixtures, for different helium flows: full squares=3500 sccm, full stars=7000 sccm, full circles=14000 sccm, full diamonds=21000 sccm, and crosses=28000 sccm.

Figure 6: Evolution versus the NO flow of the O₂(a¹Δ_g) (full diamonds) and O₃ (full squares) number densities obtained at atmospheric pressure, for a discharge current of 3 mA, in He/O₂/NO mixtures, with constant oxygen partial pressure of 10 mbar and helium flows of (a) 8000 sccm and (b) 25000 sccm.

Figure 7: Evolution versus the NO flow of the O₂(a¹Δ_g) (full diamonds) and O₃ (full squares) number densities obtained at atmospheric pressure, for a discharge current of 3 mA, in He/O₂/NO mixtures, with constant oxygen partial pressure of 20 mbar and helium flows of (a) 6250 sccm and (b) 25000 sccm.

Figure 8: Schematic of the quenching of O-atom and O₃ by NO.

Figure 9: Evolution of the O₂(a¹Δ_g) number density versus the helium flow, obtained at atmospheric pressure, for a discharge current of 3 mA, in He/O₂/NO mixtures, with constant NO flow of 1.4 sccm and different oxygen partial pressures: full squares=3 mbar, full stars=10 mbar and full circles=20 mbar.

Figure 10: Evolution of the O₂(a¹Δ_g) number density versus the discharge current, obtained at atmospheric pressure in a He/O₂/NO mixture with O₂ and NO partial pressures respectively equal to 23 and 0.19 mbar, and an helium flow of 3500 sccm.

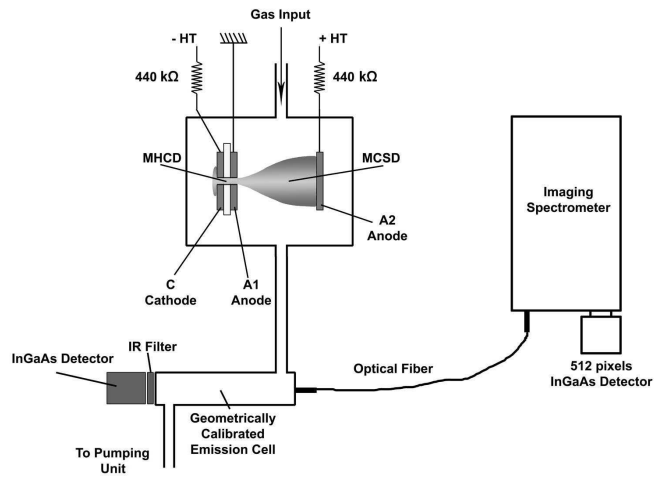


Fig. 1

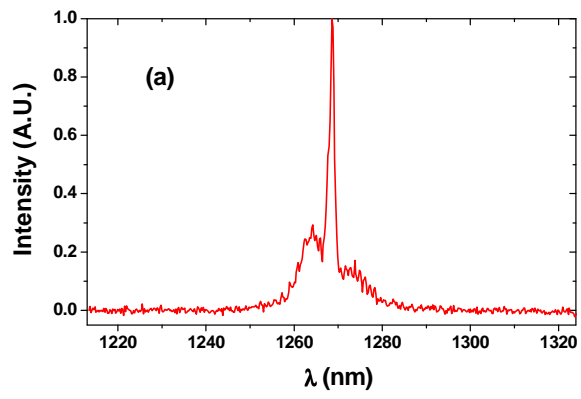


Fig. 2 (a)

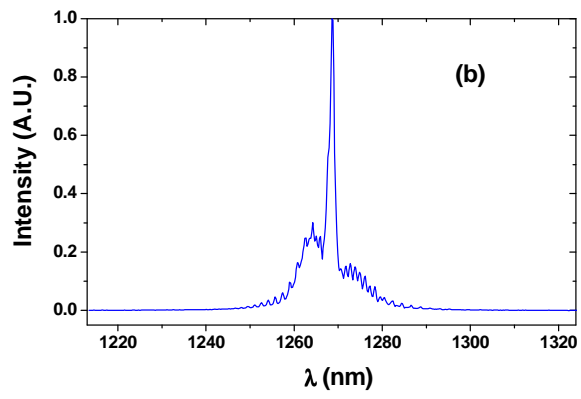


Fig. 2 (b)

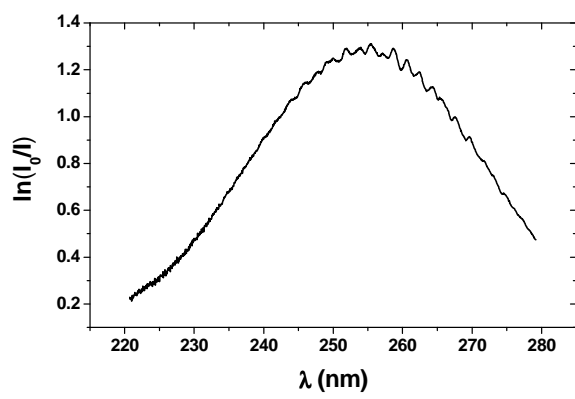


Fig. 3

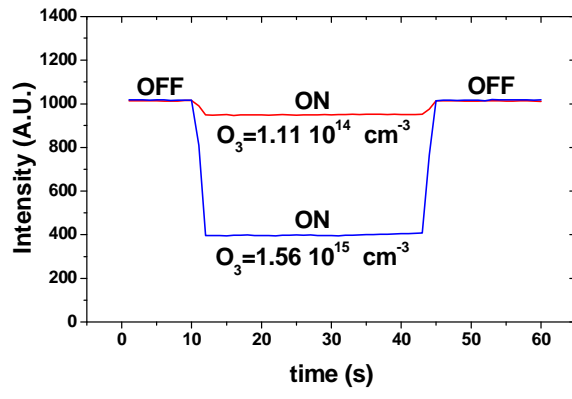


Fig. 4

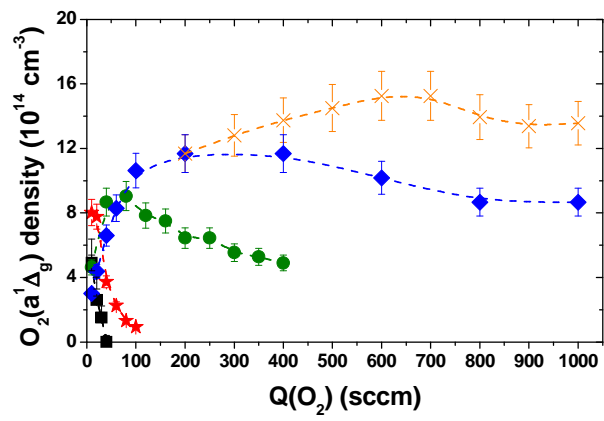


Fig. 5

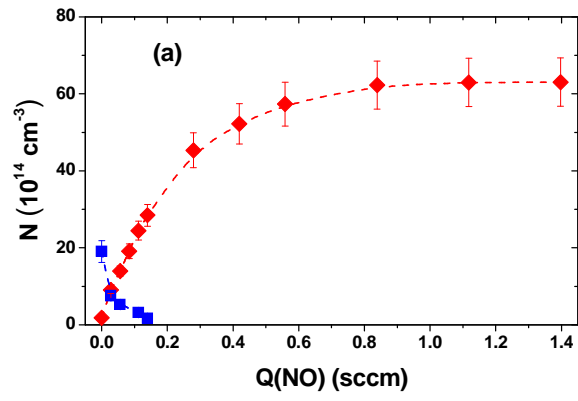


Fig. 6 (a)

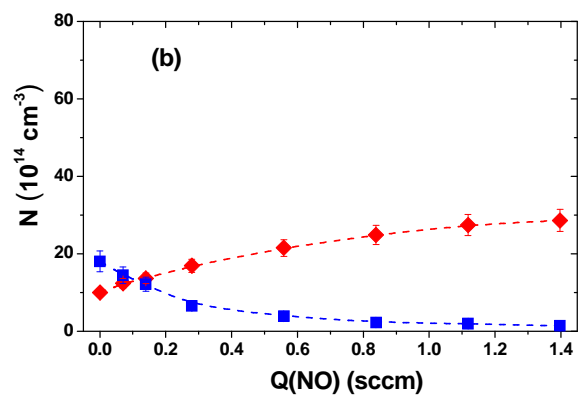


Fig. 6 (b)

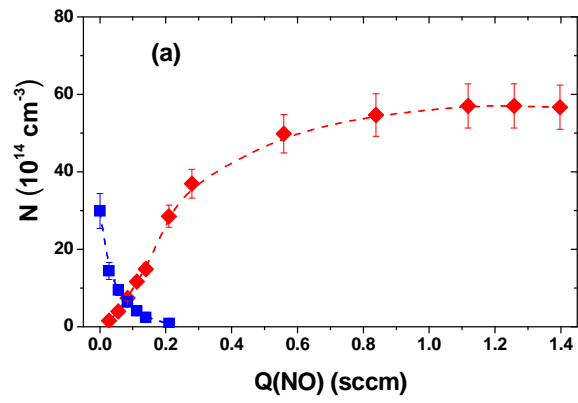


Fig. 7 (a)

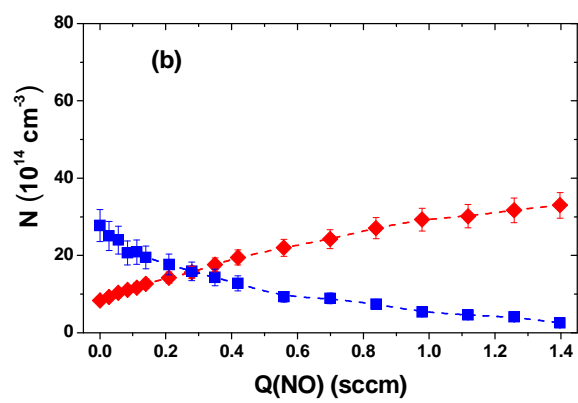


Fig. 7 (b)

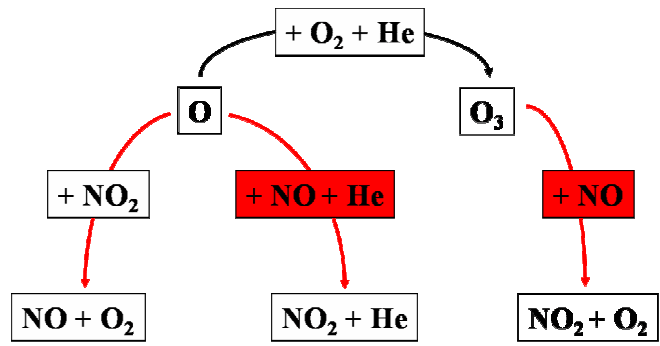


Fig. 8

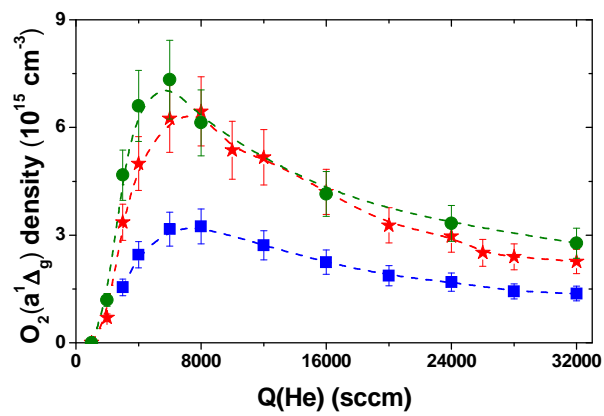


Fig. 9

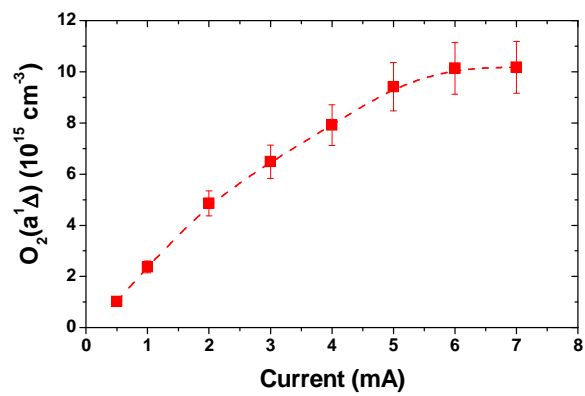


Fig. 10